Sci

MDPI

Article

Assessing the Antimicrobial Efficacy of Graphene Oxide and Its PEGylated Derivative Against *Staphylococcus aureus*

María F. Gilsanz-Muñoz [1], Mónica Martínez-Martínez [2], Javier Pérez-Piñeiro [1], Miriam Roldán [3], Mariana P. Arce [1], Rodrigo Blasco [1], Laura Rico-San Román [2], Fernando Esperón-Fajardo [2,*], Arisbel Cerpa-Naranjo [1,*] and Bárbara Martín-Maldonado [2]

1 School of Architecture, Engineering and Design, Universidad Europea de Madrid, C. Tajo s/n, Villaviciosa de Odón, 28670 Madrid, Spain; mariafuencisla.gilsanz@universidadeuropea.es (M.F.G.-M.); javier.perez4@universidadeuropea.es (J.P.-P.); mariana.arce@universidadeuropea.es (M.P.A.); rodrigo.blasco@universidadeuropea.es (R.B.)
2 School of Biomedical and Health Sciences, Universidad Europea de Madrid, C. Tajo s/n, Villaviciosa de Odón, 28670 Madrid, Spain; monica.martinez@universidadeuropea.es (M.M.-M.); laura.rico@universidadeuropea.es (L.R.-S.R.); barbara.martin-maldonado@universidadeuropea.es (B.M.-M.)
3 Professional Formation Centre, Universidad Europea de Madrid, C. Tajo s/n, Villaviciosa de Odón, 28670 Madrid, Spain; miriam.roldan@universidadeuropea.es
* Correspondence: fernando.esperon@universidadeuropea.es (F.E.-F.); arisbel.cerpa@universidadeuropea.es (A.C.-N.)

Abstract: The rise of antimicrobial resistance (AMR) has become a critical health challenge. This, plus the antimicrobial discovery void, had led scientists to search for an effective alternative to antimicrobials. In this context, nanomaterials, such as graphene oxide (GO), a two-dimensional (2D) carbon molecule with oxidized functional groups, have been shown to interact physically and chemically with bacteria. Moreover, the addition of polyethylene glycol (PEG) to its surface enhances GO's biocompatibility and water solubility, making it a promising candidate for biomedical applications. This study evaluates the antimicrobial efficacy of GO and its polyethylene glycol-modified form (GO-PEG) against *Staphylococcus aureus*, a bacterium responsible for numerous hospital-acquired and multidrug-resistant infections. After their production, both nanomaterials were characterized using various techniques to provide insight into their morphology, stability, and functional group composition. Then, the antimicrobial activity of GO and GO-PEG was assessed using the Müeller–Hinton broth microdilution method, determining the minimum inhibitory concentration (MIC) for *S. aureus* among ten different concentrations of both nanomaterials (from 0.0625 to 32 mg/mL). The results demonstrate the potential of GO as an effective antimicrobial agent at 16 and 32 mg/mL, offering new strategies in the fight against AMR. Further research could establish its role in future therapeutic applications.

Keywords: nanomaterials; nanoparticles; GO; GO-PEG; antibiotics alternative; antimicrobial resistance

Citation: Gilsanz-Muñoz, M.F.; Martínez-Martínez, M.; Pérez-Piñeiro, J.; Roldán, M.; Arce, M.P.; Blasco, R.; Rico-San Román, L.; Esperón-Fajardo, F.; Cerpa-Naranjo, A.; Martín-Maldonado, B. Assessing the Antimicrobial Efficacy of Graphene Oxide and Its PEGylated Derivative Against *Staphylococcus aureus*. *Sci* **2024**, *6*, 66. https://doi.org/10.3390/sci6040066

Academic Editor: Artur M. S. Silva

Received: 13 September 2024
Revised: 18 October 2024
Accepted: 21 October 2024
Published: 24 October 2024

1. Introduction

One of the greatest current medical challenges is antimicrobial resistance (AMR). Since the discovery of penicillin in 1928 by Alexander Fleming, antibiotics have spread worldwide, becoming one of the cornerstones of modern medicine [1]. Nevertheless, the bacteria's adaptability and rapid multiplication led to AMR's emergence [2]. While the discovery of new effective antimicrobial molecules has drastically slowed down in recent decades, the detection of AMR in bacteria has exponentially increased, with a growing number of cases of infections caused by multidrug-resistant (MDR; resistant to at least three different families of antibiotics) and pan-resistant (PDR; resistant to the entire known antimicrobial spectrum) bacteria being reported in recent years [3,4]. Although any bacteria can develop AMR mechanisms, 70% of the deaths involving antimicrobial-resistant bacteria

(ARB) are due to infection by *Staphylococcus aureus*, *Escherichia coli*, *Streptococcus pneumoniae*, *Klebsiella pneumoniae*, *Acinetobacter baummanni*, and *Pseudomonas aeruginosa* (in decreasing order of prevalence) [5]. It is important to mention that 56.9% of skin infections are caused by *S. aureus*, highlighting the relevance in public health of this bacteria species [6]. At hospitals, *S. aureus* has become a clear example of the result of decades of indiscriminate use of antibiotics and represents the connection between the treatment of wounds or skin lesions with antibiotics and nosocomial infections associated with long-stay hospital patients [7]. Regarding the antimicrobial resistance phenomenon, in 2019 alone, the number of deaths caused by these superbugs exceeded 1.5 million directly, and almost 5 million indirectly worldwide [5]. These data suggest that the increase and spread of AMR have accelerated, and previous predictions may be underestimates [5,8,9]. At the same time, this health crisis has negative socioeconomic repercussions. For example, in the United States alone, AMR represents an annual economic cost of over USD 7 billion [10]. However, despite all efforts to minimize the development and spread of AMR by international agencies, such as the FDA (Food and Drug Administration), CDC (Centers for Disease Control), ECDC (European Centers for Disease Control), or EFSA (European Food Safety Authority), it remains a natural and unstoppable process. Therefore, it is necessary and urgent to find an alternative to the use of antimicrobials that is effective and safe for infection treatment.

Currently, new therapeutic strategies against bacteria are being investigated, such as the use of nanomaterials that do not promote resistance development and are effective and safe for humans and animals [11]. Carbon-based nanomaterials have significant antimicrobial activity [12], which has attracted the attention of the entire scientific community. Among them, graphene oxide (GO) is one of the most commonly used. GO has a two-dimensional (2D) structure with hexagonally distributed carbon atoms and contains various oxidized functional groups, which improve its dispersion and stability. Moreover, it is highly recommended for biomedical applications due to its large surface area, high dispersibility, good colloidal stability, easy surface modification, and good biocompatibility [13]. The antimicrobial activity of GO is supposed to be effective against both Gram-negative and Gram-positive bacteria, due to the physical and chemical interactions that take place when GO layers come into direct contact with bacterial cells [14,15]. Nonetheless, the antimicrobial activity of nanoparticles depends on their composition, surface modification, intrinsic properties, and the type of microorganism [16]. Moreover, the addition of polyethylene glycol (PEG) to the GO molecule improves its biocompatibility and solubility in water [17].

This study aimed to assess the antimicrobial potential of GO and GO-PEG against *Staphylococcus aureus*. To this end, both nanomaterials were designed, synthesized, and characterized before their antimicrobial activity analysis. Nanomaterial characterization included transmission electron microscopy (TEM), scanning electron microscopy (SEM), and atomic force microscopy (AFM), thermogravimetric analysis (TGA), derivate thermogravimetric (DTG), UV–Vis spectra, and zeta potential. Moreover, the microdilution method in Müeller–Hinton broth assessed antimicrobial activity, a standardized technique to define antimicrobial susceptibility.

2. Materials and Methods

2.1. Synthesis of PEGylated Graphene Oxide (GO-PEG)

For the PEGylation of GO, 4-arm-PEG5K-NH2 was used as the PEG coupling reagent, whereas 1-ethyl-3-(3-dimethylaminopropyl)carbodiimide hypochlorite (EDC-HCl) was employed as the carboxyl activating reagent to allow amide bond formation. A precursor of GO with a specific surface area of 20–35 m^2/g and a median mesoporous pore diameter of 127.5 Å was provided by NanoInnova Technologies S.L. (Madrid, Spain). EDC-HCl and 4-arm-PEG5K-NH_2 were purchased from Sigma-Aldrich (Madrid, Spain). All materials were used as received unless otherwise indicated. The GO-PEG was synthesized by a modification of the method reported by [18] (Figure 1).

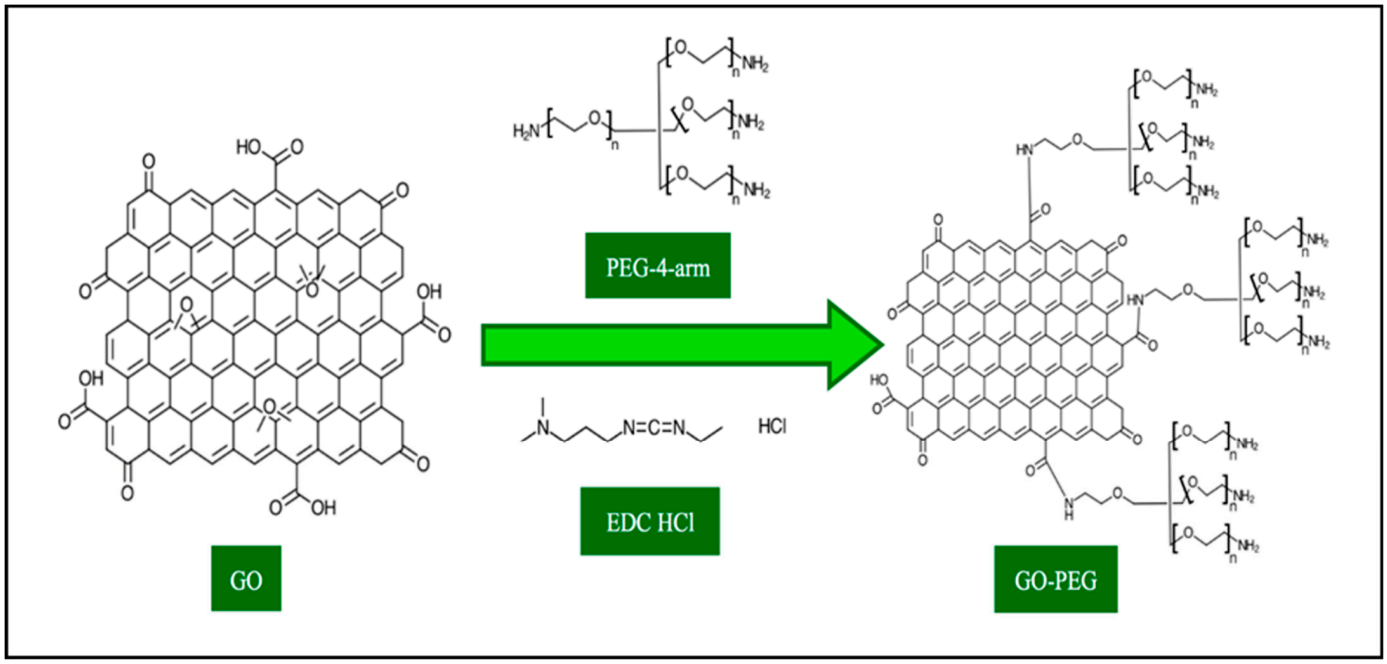

Figure 1. Scheme of the PEGylation from GO. Reproduced from [19] Cheong et al., 2020.

A mixture of 100 mg of GO and 300 mg of 4-arm-PEG-NH_2 was suspended in 100 mL of deionized water, which was bath-sonicated for 5 min. This was followed by the addition of 30 mg of EDC-HCl, and the mixture was bath-sonicated for a further 40 min at room temperature. This was followed by a further addition of 80 mg of EDC-HCl, and the mixture was stirred overnight. The resulting crude reaction mixture was centrifugated at 5000 rpm to remove unreacted PEG molecules. The pellet was subsequently washed and filtered under a vacuum. Finally, the PEGylated product was filtered to dryness under reduced pressure and then air-dried for 24 h at room temperature.

2.2. Characterization of GO and GO-PEG

A complete characterization of GO and GO-PEG was performed using different techniques. Information on their morphological surface was obtained by TEM, SEM, and AFM.

SEM images were acquired using a JEOL JSM 6335F microscope (JEOL Ltd., Tokyo, Japan), where one drop of diluted suspension of each nanoparticle sample was placed on a silicon wafer which was attached to an aluminum sample stub with a conductive carbon adhesive. TEM images of GO and GO-PEG were obtained using a JEM-2100 microscope (JEM Ltd., Tokyo, Japan), where a few drops of a diluted suspension of each nanomaterial were placed on a copper grid and allowed to dry, and AFM images were then acquired using an AFM multimode Nanoscope III A microscope (Bruke, Karlsruhe, Germany). A few drops of a diluted suspension of each nanomaterial were placed on freshly cleaved mica surface through the drop-casting method and then dried.

TGA and DTG were performed to determine how the nanoparticles can be affected by temperature. The TGA Q500 thermogravimetric analyzer (TA instruments, Barcelona, Spain) was used in a range of temperatures between 20 and 1000 °C with argon as an inert atmosphere.

UV–Vis spectra were obtained using a UV–Vis spectrophotometer Jasco V-730 (Madrid, Spain) that measured the absorption intensity of a sample by directing a laser with a range of wavelengths (λ) from the visible, ultraviolet, and infrared spectra. Absorption is directly linked to the type of state transitions and the probability of their occurrence, providing information about the molecular structure. Zeta potential values of the samples in water were acquired by a Zetasizer Nano ZS (Malvern, UK) connected to an MP-2 autotitrator (Malvern, UK), which provides information about the surface charge of the nanoparticles

and, therefore, is a measure of nanoparticle stability. To assess the value of the zeta potential according to the pH, the use of an autotitrator was necessary.

2.3. Antimicrobial Activity Analysis of GO and GO-PEG

The antimicrobial potential of GO and GO-PEG against *Staphylococcus aureus* (ATCC 25923; Thermo Scientific®, Waltham, MA, USA) was tested according to the microdilution method in Müeller–Hinton broth, one of the most commonly used quantitative methods to define bacterial susceptibility to antimicrobials. This standardized method is currently employed to assess the efficacy of antibiotic treatments and calculate the minimum effective dose of molecules for neutralizing the strain [20].

Firstly, the commercial loop with *S. aureus* was streaked into a plate of Columbia agar medium with 5% sheep blood (Oxoid Ltd.®, Basingstoke, United Kingdom), and incubated at 37 ± 1 °C for 24 h. Then, a single colony was selected and stroked on a Columbia base agar plate (Oxoid Ltd.®, Basingstoke, UK) to ensure a monoclonal culture after 24 h of incubation at 37 ± 1 °C. The inoculum was suspended in 5 mL of sterile 0.8% saline solution (Thermo Scientific®, Waltham, MA, United States of America) to achieve a turbidity equivalent to 0.5 McFarland. Subsequently, 10 µL of the suspension was transferred onto 11 mL of Mueller–Hinton broth (Oxoid Ltd.®, Basingstoke, UK) and homogenized with a vortex to obtain a well-balanced distribution of the bacteria in the Mueller–Hinton broth. Finally, the nanomaterial was added to the mixture. Each nanomaterial (GO and GO-PEG) was tested at ten different concentrations: 0.0625, 0.125, 0.25, 0.5, 1, 2, 4, 8, 16, and 32 mg/mL. So, 20 different inoculums were prepared and homogenized with a vortex before dispensing each of them into separate wells of a 96-well plate and incubating them at 37 ± 1 °C for 24 h. Then, the minimum inhibitory concentration (MIC) was established for both nanomaterials.

Bacterial activity in the incubation products was tested by catalase reaction. To this end, a sample of each incubation product was collected and deposited onto a new plate in the same position, to which 10 µL of hydrogen peroxide (H_2O_2) was added to each new well. As a catalase-positive bacterium, if *S. aureus* were alive, they would react by producing bubbles on the surface. At the same time, the bacterial viability was assessed. A sample from each incubation product was collected and streaked on Columbia base agar plates (Oxoid Ltd.®, Basingstoke, UK). The plates were incubated at 37 ± 1 °C for 24 h to determine if the bacteria's ability to multiply and create new colonies has been affected by the presence of nanomaterials at different concentrations.

All the analyses were repeated four times to ensure laboratory good practices and the repeatability of the technique. Additionally, negative controls were included to ensure the quality of the results obtained. To obtain the negative control, 0.5 McFarland *Staphylococcus* was transferred onto Mueller–Hinton broth and processed as the rest of the inoculums but without nanomaterial.

No statistical analyses were performed.

3. Results and Discussion

3.1. Characterization of Nanomaterials

The GO and GO-PEG nanomaterials were characterized using various techniques, as mentioned earlier. FTIR provided information about bond energies, thus allowing the characterization of the bonds contained in the synthesized nanomaterials. In one of our previous papers, [19] described the results obtained using this technique [18]. The FTIR spectrum of GO showed two vibrational bands at 1105 and 1732 cm^{-1}, corresponding to the C–OH and C=O stretches from the carboxylic acid group (–COOH) within the graphitic structure. The band resonating at 1622 cm^{-1} was considered the bending mode in the sp^2 hybridized C=C within the highly conjugated GO structure. The broad signal observed between 3500–3000 cm^{-1} can be attributed to OH stretching due to intermolecular hydrogen bond interactions. The shift of the peak from 1622 cm^{-1} to 1650 cm^{-1} indicates that PEG has been correctly attached to graphene oxide [19].

The morphological structure of the studied samples was determined by TEM and SEM techniques. Figure 2a displays the smooth and transparent surface that GO presented. The almost transparent wrinkled sheet-like structure of GO is evident from the TEM image. Some folds were observed, which is characteristic of this material. The addition of PEG produced a denser effect in the structure of the GO-PEG sample (Figure 2b). The number of folds tended to increase, and the GO-PEG sample appeared more compact and darker. Similar appearances were observed in the SEM images (Figure 2c,d). The SEM image of GO showed a sheet-like structure with a partially wrinkled and wavy surface, while the GO-PEG sample appeared more compact. The conjugation of PEG to GO led to an increase in the size of the nanomaterial as viewed under an accelerating voltage of 20 KV. PEG was found to be embedded in GO sheets, thus resulting in the formation of a matrix-like structure. These findings agree with the ones observed by other researchers [21,22].

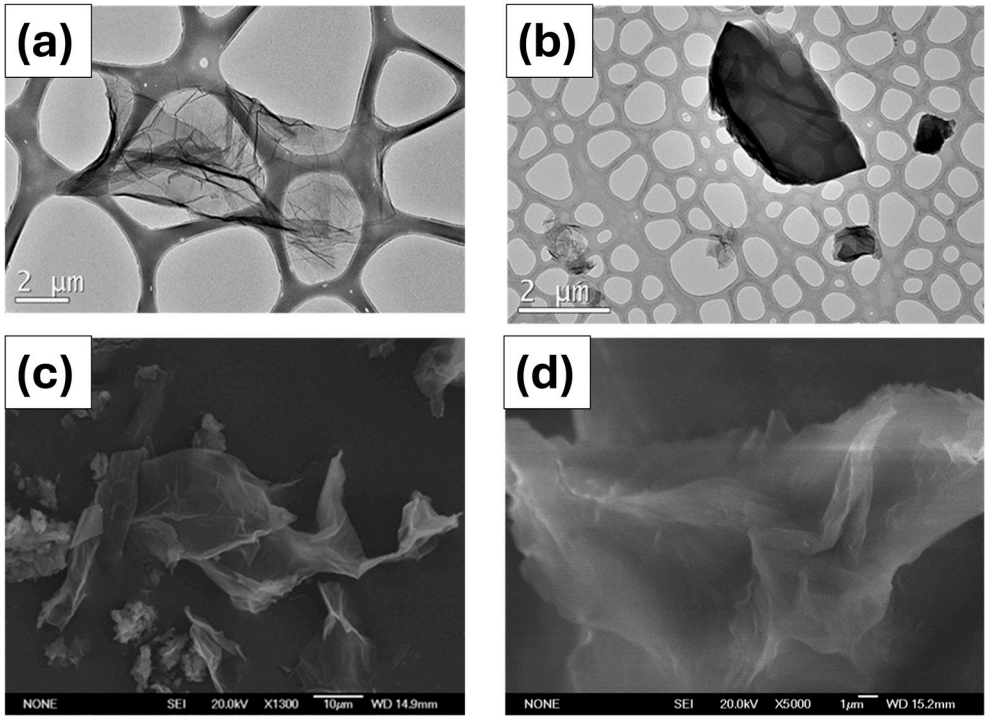

Figure 2. TEM and SEM images of GO (**a**,**c**) and GO-PEG (**b**,**d**), respectively.

The morphology of GO and GO-PEG was recorded by AFM, as illustrated in Figures 3 and 4, and described by Zeer et al. [23]. The 2D and 3D AFM images of the GO and GO-PEG samples dispersed in water provide information on the height profile, surface roughness, and average height of the samples. The nanomaterial surface significantly influences the interaction with bacteria. The line represented in Figure 3A demonstrates the height profile for each particle of GO. The height values obtained were between 10–140 nm. The average height of the peaks observed in the Z axis was determined to be 11.88 nm, with a root mean square (RMS) roughness of 10.84 nm that represents the roughness distribution for the entire surface and an average roughness of 3.50 nm for GO sample (Figure 3).

Additionally, in Figure 4, the 2D and 3D images of GO-PEG and its height profile are presented. The white dashed line represented in Figure 4A shows the height profile for each particle of GO-PEG. The height obtained is between 10–110 nm. In this case, the average height in the Z axis is 18.68 nm, with an RMS surface roughness of 13.20 nm and an average roughness of 5.89 nm. When comparing these data with those obtained in Figure 3, an increase in the different parameters studied is observed, which can be attributed to the PEGylation of GO. This has been confirmed by the other techniques used in the present study to assess the characterization of GO and GO-PEG. The morphology of similar materials has also been studied by different researchers [23–26].

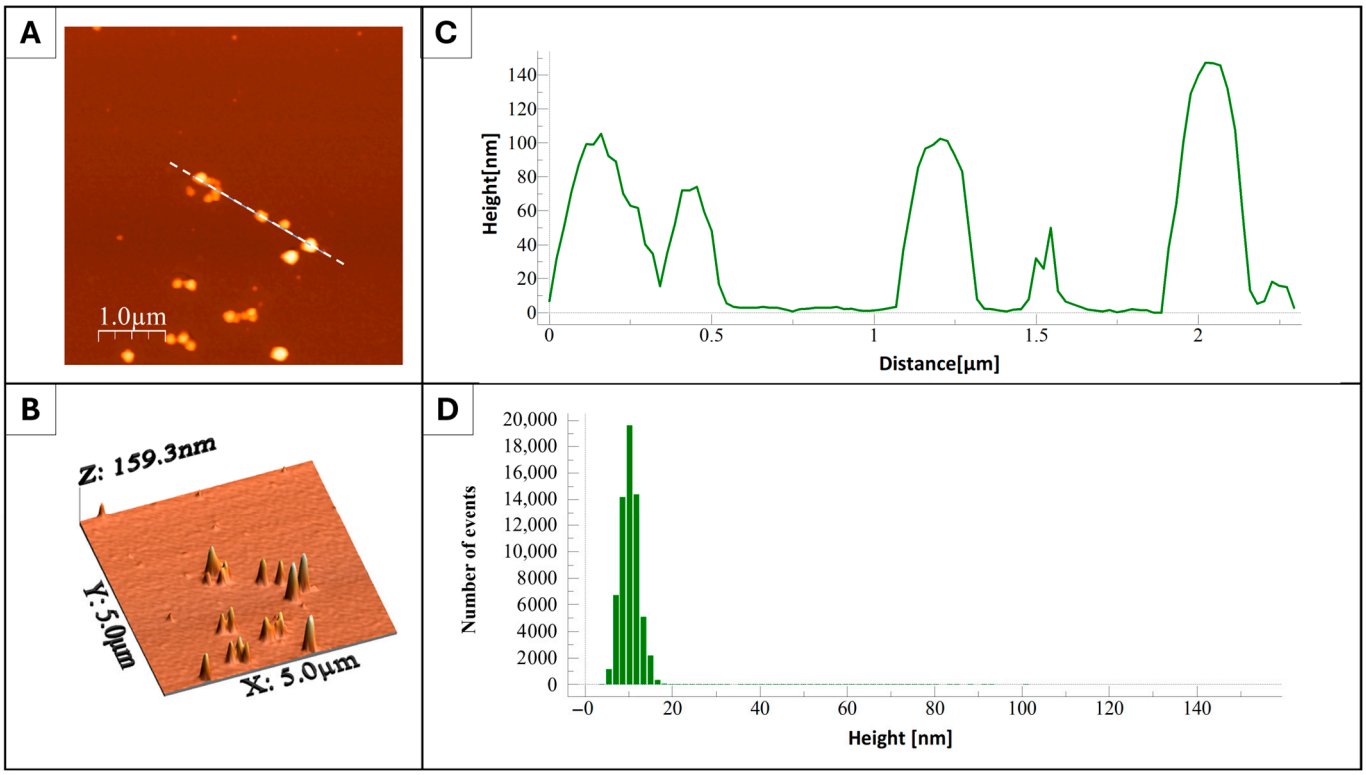

Figure 3. AFM images and results of the GO sample. (**A**) 2D representation and surface texture. (**B**) 3D morphology dispersed in water obtained by tapping mode imaging in air. (**C**) Histogram of the height profile. (**D**) Average height.

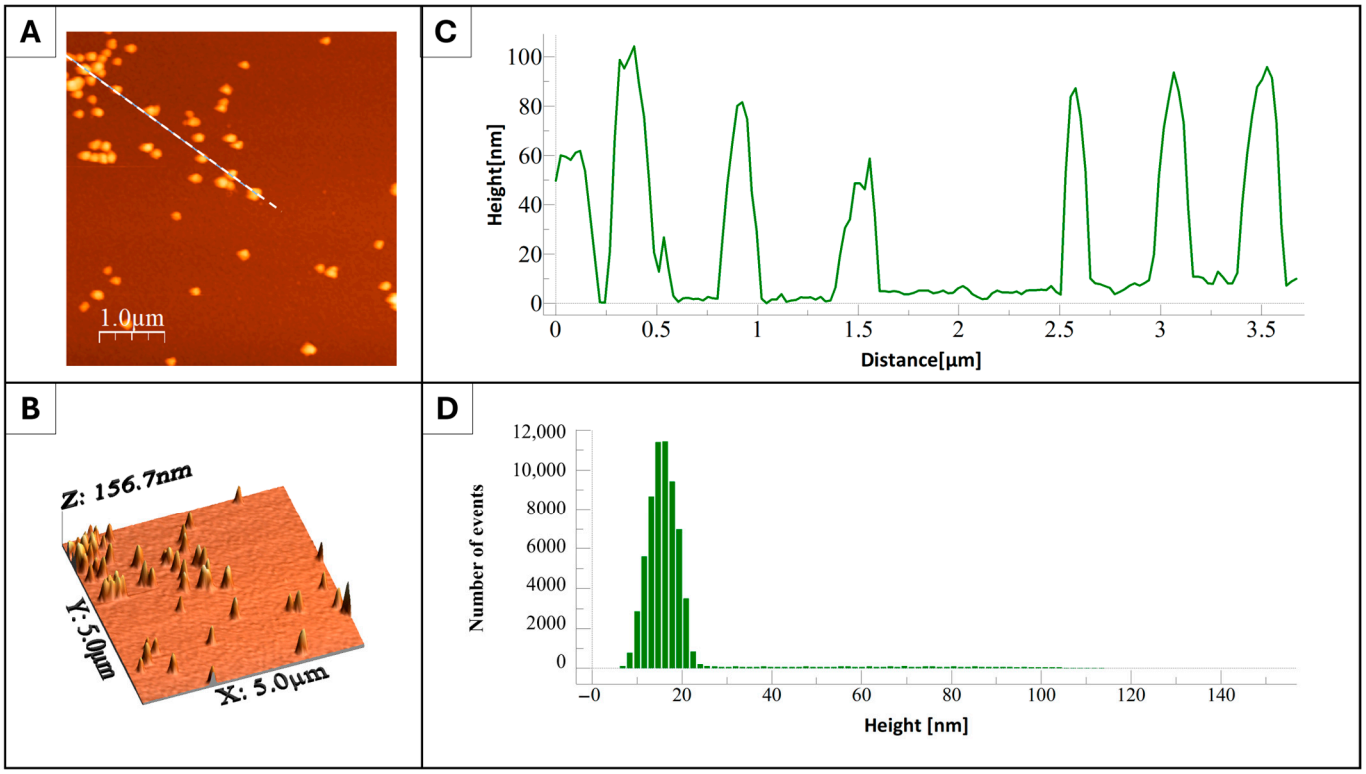

Figure 4. AFM images and results of the GO-PEG sample. (**A**) 2D representation and surface texture. (**B**) 3D morphology dispersed in water obtained by tapping mode imaging in air. (**C**) Histogram of the height profile. (**D**) Average height.

Tests of the thermal stability of the samples was carried out by thermogravimetric analysis (TGA), and the results are shown in Figure 5. TGA is commonly used to characterize materials, like GO and GO-PEG nanocomposites, and it typically involves observing weight changes in a material as it is heated. The first mass loss observed in the GO curve between the initial temperature and approximately 120 °C (12.5%) may be due to the removal of residually adsorbed and combined water, which resides in the spaces between the GO layers [22,27]. This loss decreased in the GO-PEG functionalized samples. The second loss, which occurred between 150 and 350 °C, was due to the decomposition of oxygen, hydroxyl groups, and acids groups [28]. This second loss shifted towards a higher temperature in the case of GO-PEG, where a sharp drop in weight is observed in the range 150–250 °C, with a maximum in the derivative thermogravimetric (DTG) around 205 °C. Moreover, an additional loss was detected in its TG curve, between 250 and 425 °C, which can be attributed to the oxygenated groups of the PEG.

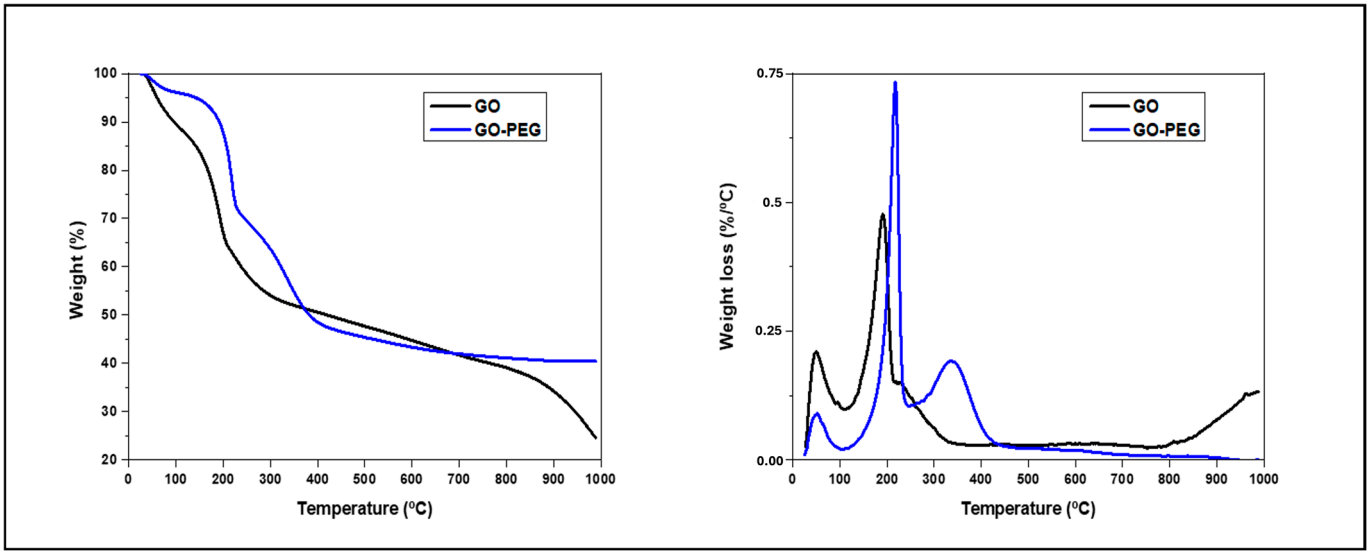

Figure 5. Thermal analysis (TGA, **left**, and DTG, **right**) curves of GO and GO-PEG samples.

TGA was mentioned as a characterization technique used to study the properties of the materials. Previous studies have reported on the TGA of GO and GO-PEG. For instance, Wang employed TGA to assess the thermal stability of a composite phase-change material (CPCM) made from GO and PEG, while Serag evaluated the thermal stability of GO-PEG-PVA composites using TGA samples [29,30]. Although the specific peaks of weight loss in the TG of GO and GO-PEG are not described, these papers collectively suggest that TGA is an important tool for evaluating the thermal behavior of GO-PEG composites, which can include the assessment of thermal stability and decomposition patterns [29,30].

At the same time, UV–Vis spectra revealed two characteristic peaks of GO in Figure 6: a maximum peak at 230 nm corresponding to the $\pi-\pi^*$ transitions of aromatic C−C bonds, and a shoulder near 300–310 nm assigned to the $n-\pi^*$ transitions of C−O bonds, whereas in the GO-PEG sample a low-intensity peak can be clearly seen at a wavelength of approximately 247 nm which is probably due to the interactions between GO and PEG, indicating successful PEGylation. Similar studies have been carried out by different researchers [23,25,26].

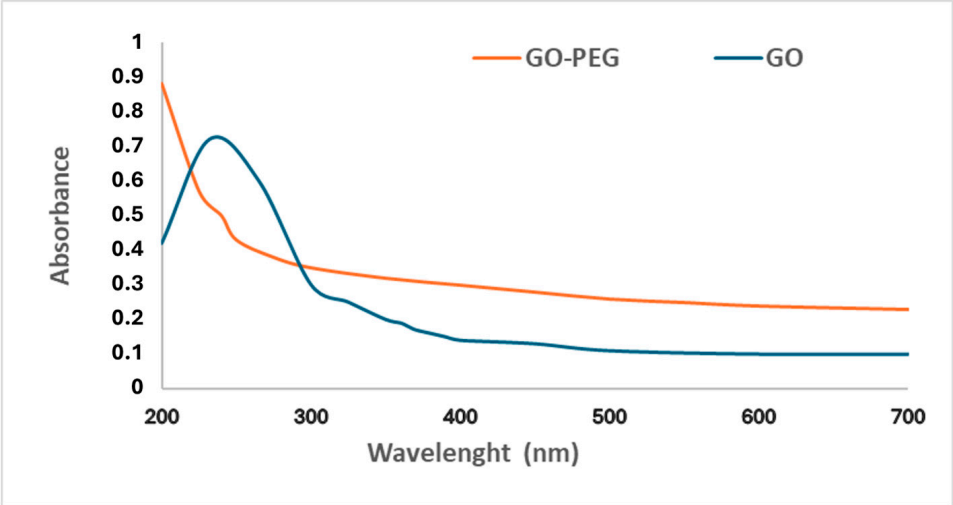

Figure 6. UV–Vis spectra of GO and GO-PEG.

The last characterization technique was the zeta potential, and measurements of GO and GO-PEG are shown in Figure 7. Samples were measured in triplicate to determine the zeta potential value as the average ± standard deviation. The zeta potential values obtained confirmed their stability at neutral pH. A significant increase from −35.4 ± 2.1 mV to −29.4 ± 2.53 mV can be observed for GO and GO-PEG, respectively, confirming the successful functionalization of PEG on the GO surface because of the amidation. GO nanosheets had a negative zeta potential, owing to the negative charge functional groups on the surface of GO sheet, such as –OH and –COOH [23]. Some authors consider ± 25 mV as a value for assuring the stability of suspensions [31]. The dispersions were stable, although certain polydispersity was detected. The zeta potential of different carbon-based materials has also been assessed in previous studies [24,25,32].

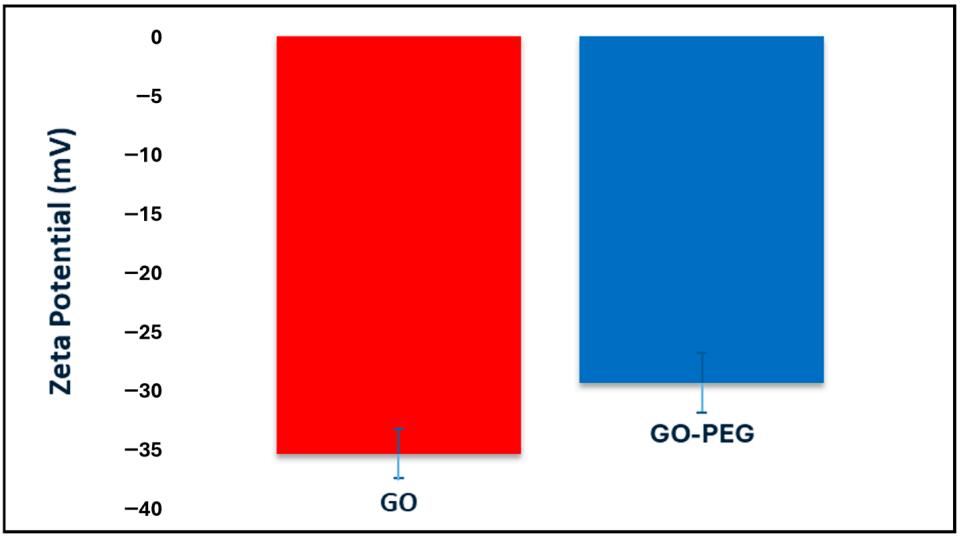

Figure 7. Zeta-potential measurement of GO and GO-PEG at pH = 6 and pH = 7.5, respectively. Samples were measured three times, and error bars indicate the standard deviation.

3.2. Antimicrobial Potential of GO and GO-PEG

The effects of ten different concentrations of GO and GO-PEG against *S. aureus* are detailed in Table 1.

Table 1. Detailed results of antimicrobial activity of GO and GO-PEG exposition for *Staphylococcus aureus*.

	Graphene Oxide (GO) Effects			PEGylated Graphene Oxide (GO-PEG) Effects		
Nanomaterial Concentration	**Antimicrobial Activity [1]**	**Catalase Reaction [2]**	**Bacterial Viability [3]**	**Antimicrobial Activity [1]**	**Catalase Reaction [2]**	**Bacterial Viability [3]**
32 mg/mL	+	−	−	−	+	+
16 mg/mL	+	−	−	−	+	+
8 mg/mL	−	+	+	−	+	+
4 mg/mL	−	+	+	−	+	+
2 mg/mL	−	+	+	−	+	+
1 mg/mL	−	+	+	−	+	+
0.5 mg/mL	−	+	+	−	+	+
0.25 mg/mL	−	+	+	−	+	+
0.125 mg/mL	−	+	+	−	+	+
0.0625 mg/mL	−	+	+	−	+	+

[1] +: no growth at the bottom of the well after incubation; −: growth. [2] +: positive reaction, so live bacteria on the incubated inoculums; −: negative reaction, no viable bacteria. [3] +: positive reaction from the incubated inoculums; −: negative reaction.

In summary, the results demonstrated the effectiveness of GO as an antimicrobial agent against *S. aureus* at high concentrations, with an MIC of 16 mg/mL. In consequence, *S. aureus* was unable to multiply and produce colonies in the presence of GO at 16 and 32 mg/mL. Additional tests (catalase reaction and Columbia base agar subcultures) were consistent with those reported above. The catalase reaction was negative in the incubated inoculums exposed to 16 and 32 mg/mL of GO (Figure 8). Regarding the subcultures, all the incubated GO inoculums contained bacteria able to develop visible colonies except those exposed to GO at concentrations of 16 and 32 mg/mL. The results of the quadruplicate analyses were similar, confirming our experiment's reliability and reproductivity.

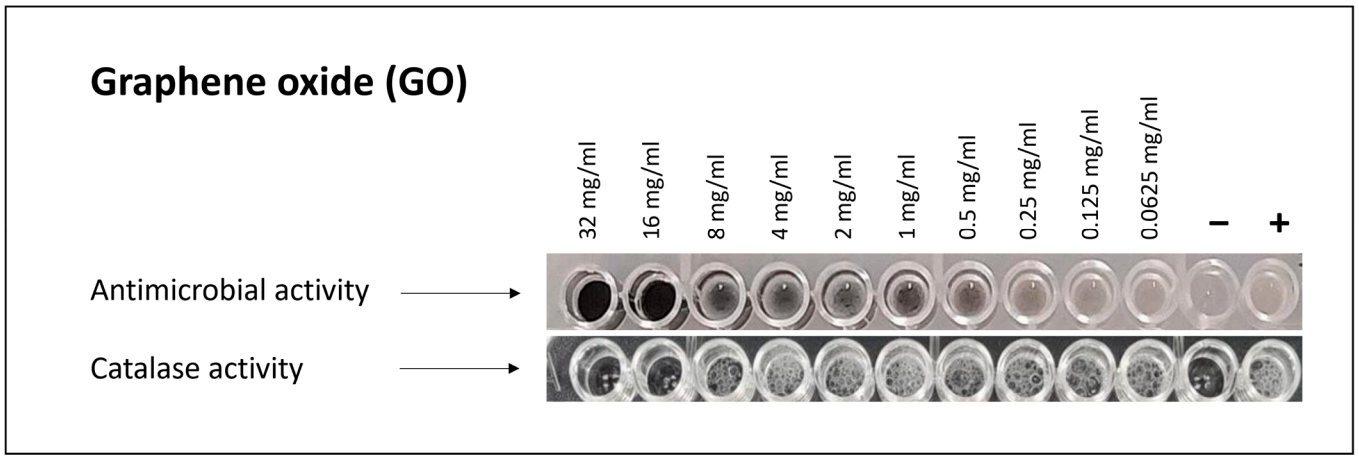

Figure 8. Results of the incubation of GO inoculums at ten different concentrations and respective catalase reactions. Note that the color of the inoculums with nanomaterial was black, while the bacterial colonies and the foam produced by the positive reaction of catalase were white. Therefore, the darker wells are those in which there has been no bacterial growth, and, therefore, the nanomaterial is effective at this concentration.

According to our results, the effectiveness of GO has been described as concentration-dependent, so the determination of MIC is vital to ensure the minimal effective dose at lower costs [33]. Most of the previous studies published about the antimicrobial ability of graphene oxide have been performed according to the Kirby–Bauer or disc-diffusion method [34–36]. However, this method has been described as a qualitative method for antimicrobial susceptibility assessment, in which the correlation between zone diameters and resistance is possible due to the standardization of the method. pH, ion concentration and agar depth of Müeller–Hinton plates are key factors for accurate results. In contrast, microdilution in Müeller–Hinton broth is a quantitative method, so it permits the determination of the MIC for each antimicrobial agent [37]. In our study, the MIC was 16 mg/mL for GO, contrasting with the MIC reported at 0.2 mg/mL against *S. aureus* isolated from bovine mastitis [38]. This difference could be due to two possibilities. First, the inoculums were prepared differently in both experiments. Our experiment was based on a bacterial solution at 0.5 McFarland turbidity, which assumes a bacterial population of 1.5×10^8 CFU/mL [39]. The McFarland scale has been widely employed in antimicrobial susceptibility testing worldwide and nowadays has become the standard technique. In the bovine mastitis study, bacterial inoculums were prepared with bacterial suspensions of 1×10^6 CFU/mL, a significantly lower proportion of bacteria [38]. The difference in bacterial proportion could lead to different MICs to achieve the destruction of all the bacteria. Moreover, the solvent employed for the inoculums can be a key factor in the antimicrobial effectiveness of GO. Not all the solvents allow the GO antimicrobial activity, probably due to the nanoparticles' interaction with the medium's molecules [40]. In this sense, the saline solution seems to be the better solvent, while others, like PBS, Luria Bertani broth, or DMEM, are not suitable for this application [38]. The composition of Müeller–Hinton broth can vary between different brands and manufacturers, but the concentration of divalent cations, such as Ca^{2+} and Mg^{2+}, tends to be high in the best brands [41]. These divalent cations can cause GO nanoparticles aggregation impacting on the GO antimicrobial activity [42]. So, the use of Müeller–Hinton broth instead of the saline solution could also explain the difference between our MIC (16 mg/mL) and the one reported by Saeed et al. [38]. Further studies were needed to confirm our theory, comparing the use of Müeller–Hinton broth and saline solution as solvents in the preparation of the inoculums.

Multidrug-resistant *S. aureus* infection treatments remain a challenge in both human and veterinary medicine. Previous studies have demonstrated the synergy of GO when applied with different antibiotics or other molecules, such as metals or curcumin [33,35,43]. Some of them have evaluated the possible GO antimicrobial mechanisms. Among them, the most recognized are the envelope of the bacteria and restriction of nutrient acquisition, the impact on membrane and cytoskeleton structure and functions, the triggering of oxidative stress, or mechanical destruction of the bacterial membrane [34,44–47]. The latter would allow the GO to reach and kill intracellular bacteria [38]. Unfortunately, mammalian cells can also be affected by GO nanoparticles, and cytotoxicity has been reported in in vitro experiments [38,42]. For example, a study confirmed 50–70% fibroblast vitality reduction and up to 90% hemolysis after 24 h of 0.05 mg/mL GO–curcumin exposure [43]. In vivo experiments in mice reported platelet depletion, pro-inflammatory response, lung and liver lesions, such as granulomas, loss of body weight, and even death [45,48–50].

Within this framework, the addition of PEG to the pristine GO molecule improves the biocompatibility and safety of this nanomaterial for medical applications [45]. However, regarding our GO-PEG analyses, the PEGylated modification of GO failed as an antimicrobial against *S. aureus* at the concentrations tested. The bacteria could multiply and create colonies at the bottom of the plate, and the incubated inoculums have positive catalase reactions, confirming that the bacteria present in those wells were still alive (Figure 9).

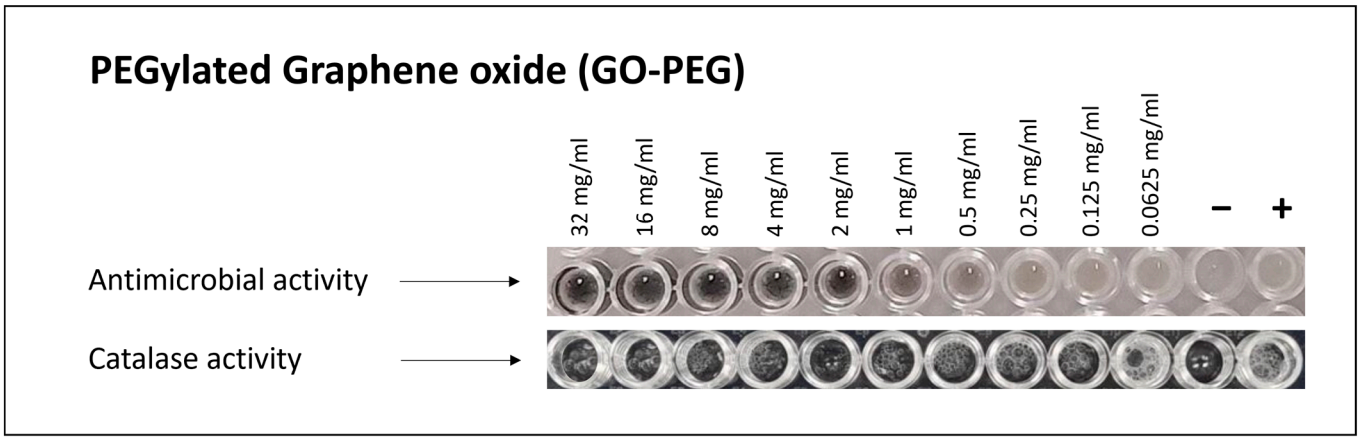

Figure 9. Results of the incubation of GO-PEG inoculums at ten different concentrations and respective catalase reactions. Note that the color of the inoculums with nanomaterial was black, while the bacterial colonies and the foam produced by the positive reaction of catalase were white. Therefore, the darker wells are those in which there has been no bacterial growth, and, therefore, the nanomaterial is effective at this concentration.

The addition of PEG compound to the GO molecule leads to a bigger molecule, as represented in Figure 1, and it is important to highlight the wide variety in sizes of PEG molecules available on the market. So, the bigger the PEG compound, the bigger the GO-PEG molecule will be. Some of the antimicrobial mechanisms described for GO depend on the internalization of the molecule or the interaction between GO molecules and bacteria [34,44,46]. For the first case, if the PEGylated modification is bigger, the transport or endocytosis of the molecules through the membrane cell could be complicated. For the second, as PEG recovers the GO surface, the interaction between GO and the bacteria could be blocked. Therefore, the inefficacy of GO-PEG as an antimicrobial observed in our experiment may be attributed to the surface modification of the nanoparticles. It is highly likely that, in some way, increasing the biocompatibility of GO with eukaryotic cells through PEGylation will also enhance its biocompatibility with prokaryotic cells and then with bacteria. However, previous studies reported that the PEGylated modification of GO nanocomposites with silver (GO-PEG-Ag) or other molecules demonstrated some antimicrobial activity with lower cytotoxicity at in vitro conditions [51,52]. Reducing the size of the GO sheets might increase the surface/volume ratio, internalization, and direct physical damage to the bacterial membrane, maximizing cell contact and increasing the effectiveness of the material. Also, the combination of GO with metal nanoparticles (i.e., silver or copper) can lead to a strategical synergy to increase antibacterial efficacy. In this context, much research is still needed about nanomaterial applications in medicine to obtain an effective, safe, and economically viable alternative to antibiotics.

4. Conclusions

Graphene oxide (GO) exhibited antimicrobial properties against *S. aureus*, and was able to inhibit its metabolic activity, multiplication, and colonization. The minimum inhibitory concentration of GO was 16 mg/mL, significantly higher than previous studies, due to inoculum preparation or the employment of Müeller–Hinton broth. Although it is the standard medium for antimicrobial susceptibility tests, Müeller–Hinton broth could be a non-suitable solvent for GO antimicrobial activity assessments. This highlights the need to standardize an antimicrobial susceptibility method suitable for nanomaterials. Finally, the PEGylation of graphene oxide (GO-PEG) showed no advantage in the antimicrobial activity against *S. aureus*. Therefore, further research is needed to understand the intrinsic mechanisms of the antimicrobial activity of GO and to find a biocompatible modification for medical applications.

Author Contributions: Conceptualization, F.E.-F., A.C.-N., B.M.-M., and J.P.-P.; methodology, M.F.G.-M., M.M.-M., M.R., M.P.A., R.B., A.C.-N., B.M.-M., and J.P.-P.; software, J.P.-P. and A.C.-N.; validation, M.F.G.-M., M.M.-M., and B.M.-M.; formal analysis, A.C.-N., B.M.-M., and J.P.-P.; investigation, A.C.-N., L.R.-S.R., M.F.G.-M., M.M.-M., and B.M.-M.; resources, A.C.-N., F.E.-F., and B.M.-M.; writing—original draft preparation, B.M.-M., J.P.-P., and A.C.-N.; writing—review and editing, L.R.-S.R., M.R., and M.F.G.-M.; visualization, A.C.-N. and B.M.-M.; supervision, A.C.-N. and B.M.-M.; project administration, B.M.-M.; funding acquisition, A.C.-N., F.E.-F., and B.M.-M. All authors have read and agreed to the published version of the manuscript.

Funding: This research was funded by SANTANDER UNIVERSIDADES and the FUNDACIÓN UNIVERSIDAD EUROPEA, grant number XSAN002302.

Institutional Review Board Statement: Not applicable.

Informed Consent Statement: Not applicable.

Data Availability Statement: The data presented in this study are available on request from the corresponding author due to legal restrictions.

Acknowledgments: The authors would like to thank Rojas-Cervantes, from the Universidad Nacional de Educación a Distancia (UNED), Madrid, Spain, for her collaboration in performing the TGA/DTG analyses.

Conflicts of Interest: The authors declare no conflicts of interest.

References

1. Bennett, J.W.; Chung, K.T. Alexander Fleming and the discovery of penicillin. *Adv. Appl. Microbiol.* **2001**, *49*, 163–184. [CrossRef] [PubMed]
2. Iglesias, J.O. Comprendiendo la resistencia a antibióticos. *Rev. De Investig. Y Educ. En Cienc. De La Salud* **2019**, *4*, 84–89. [CrossRef]
3. Muñoz, C. *Módulo I: Generalidades. Jornada Formativa Sobre la Resistencia a los Antibióticos. Plan Nacional de Resistencias Frente a Antibióticos*; Colegio Oficial de Veterinarios de Madrid: Madrid, España, 2017.
4. Jiménez, M.A.; Galas, M.; Corso, A.; Hormazábal, J.C.; Duarte Valderrama, C.; Salgado Marcano, N.; Ramón-Pardo, P.; Melano, R.G. Consenso latinoamericano para definir, categorizar y notificar patógenos multirresistentes, con resistencia extendida o panresistentes. *Rev. Panam. Salud. Publica* **2019**, *43*.
5. Murray, C.J.; Ikuta KSSharara, F.; Swetschinski, L.; Aguilar, G.R.; Gray, A.; Han, C.; Bisignano, C.; Rao, P.; Wool, E. Global burden of bacterial antimicrobial resistance in 2019: A systematic analysis. *Lancet* **2022**, *399*, 629–655. [CrossRef]
6. Upreti, N.; Rayamajhee, B.; Sherchan, S.P.; Choudhari, M.K.; Banjara, M.R. Prevalence of methicillin resistant Staphylococcus aureus, multidrug resistant and extended spectrum β-lactamase producing gram negative bacilli causing wound infections at a tertiary care hospital of Nepal. *Antimicrob. Resist. Infect. Control* **2018**, *7*, 121. [CrossRef]
7. Bassetti, M.; Righi, E.; Vena, A.; Graziano, E.; Russo, A.; Peghin, M. Risk stratification and treatment of ICU-acquired pneumonia caused by multidrug-resistant/extensively drug-resistant/pandrug-resistant bacteria. *Curr. Opin. Crit. Care* **2018**, *24*, 385–393. [CrossRef]
8. Lai, C.C.; Chen, S.Y.; Ko, W.C.; Hsueh, P.R. Increased antimicrobial resistance during the COVID-19 pandemic. *Int. J. Antimicrob. Agents* **2021**, *57*, 106324. [CrossRef]
9. O'Neill, J.I.M. Antimicrobial resistance: Tackling a crisis for the health and wealth of nations. *Rev. Antimicrob. Resist* **2014**, *20*, 1–16.
10. Armbruster, W.J.; Roberts, T. The political economy of US antibiotic use in animal feed. *Food Saf. Econ. Incent. A Safer Food Supply* **2018**, 293–322. [CrossRef]
11. Ghosh, C.; Sarkar, P.; Issa, R.; Haldar, J. Alternatives to conventional antibiotics in the era of antimicrobial resistance. *Trends Microbiol.* **2019**, *27*, 323–338. [CrossRef]
12. Hu, W.; Peng, C.; Luo, W.; Lv, M.; Li, X.; Li, D.; Huang, Q.; Fan, C. Graphene-based antibacterial paper. *ACS Nano* **2010**, *4*, 4317–4323. [CrossRef] [PubMed]
13. Yin, D.; Li, Y.; Lin, H.; Guo, B.; Du, Y.; Li, X.; Jia, H.; Zhao, X.; Tang, J.; Zhang, L. Functional graphene oxide as a plasmid-based Stat3 siRNA carrier inhibits mouse malignant melanoma growth in vivo. *Nanotechnology* **2013**, *24*, 105102. [CrossRef] [PubMed]
14. Palmieri, V.; Bugli, F.; Lauriola, M.C.; Cacaci, M.; Torelli, R.; Ciasca, G.; Conti, C.; Sanguinetti, M.; Papi, M.; De Spirito, M. Bacteria meet graphene: Modulation of graphene oxide nanosheet interaction with human pathogens for effective antimicrobial therapy. *ACS Biomater. Sci. Eng.* **2017**, *3*, 619–627. [CrossRef]
15. Olivi, M.; Alfè, M.; Gargiulo, V.; Valle, F.; Mura, F.; Di Giosia, M.; Rapino, S.; Palleschi, C.; Uccelletti, D.; Fiorito, S. Antimicrobial properties of graphene-like nanoparticles: Coating effect on *Staphylococcus aureus*. *J. Nanoparticle Res.* **2016**, *18*, 1–10. [CrossRef]
16. Dizaj, S.M.; Mennati, A.; Jafari, S.; Khezri, K.; Adibkia, K. Antimicrobial activity of carbon-based nanoparticles. *Adv. Pharm. Bull.* **2015**, *5*, 19.

17. Manasrah, A.D.; Laoui, T.; Zaidi, S.J.; Atieh, M.A. Effect of PEG functionalized carbon nanotubes on the enhancement of thermal and physical properties of nanofluids. *Exp. Therm. Fluid Sci.* **2017**, *84*, 231–241. [CrossRef]
18. Zhu, S.; Zhen, H.; Li, Y.; Wang, P.; Huang, X.; Shi, P. PEGylated graphene oxide as a nanocarrier for podophyllotoxin. *J. Nanoparticle Res.* **2014**, *16*, 1–11. [CrossRef]
19. Cheong, Y.K.; Arce, M.P.; Benito, A.; Chen, D.; Luengo Crisostomo, N.; Kerai, L.V.; Rodrígez, G.; Valverde, J.L.; Vadalia, M.; Cerpa-Naranjo, A.; et al. Synergistic antifungal study of PEGylated graphene oxides and copper nanoparticles against *Candida albicans*. *Nanomaterials* **2020**, *10*, 819. [CrossRef]
20. Marroki, A.; Bousmaha-Marroki, L. Antibiotic Resistance Diagnostic Methods for Pathogenic Bacteria. In *Encyclopedia of Infection and Immunity*; Elsevier: Amsterdam, The Netherlands, 2022; Volume 4, pp. 320–341, ISBN 9780323903035. [CrossRef]
21. Deb, A.; Vimala, R. Camptothecin loaded graphene oxide nanoparticle functionalized with polyethylene glycol and folic acid for anticancer drug delivery. *J. Drug Deliv. Sci. Technol.* **2017**, *43*, 333–342. [CrossRef]
22. Jose PP, A.; Kala, M.S.; Joseph, A.V.; Kalarikkal, N.; Thomas, S. Reduced graphene oxide/silver nanohybrid as a multifunctional material for antibacterial, anticancer, and SERS applications. *Appl. Phys. A* **2020**, *126*, 58. [CrossRef]
23. Zeer, Q.; Jun, S.; Zhang, Z.; Cao, Y.; Li, J.; Cao, S. PEGylated graphene oxide-capped gold nanorods/silica nanoparticles as multifunctional drug delivery platform with enhanced near-infrared responsiveness. *Mater. Sci. Eng. C* **2019**, *104*, 109889. [CrossRef]
24. Cerpa-Naranjo, A.; Pérez-Piñeiro, J.; Navajas-Chocarro, P.; Arce, M.P.; Lado-Touriño, I.; Barrios-Bermúdez, N.; Moreno, R.; Rojas-Cervantes, M.L. Rheological properties of different Graphene nanomaterials in biological media. *Materials* **2022**, *15*, 3593. [CrossRef] [PubMed]
25. Pérez-Piñeiro, J.; Sánchez-Cea, F.; Arce, M.P.; Lado-Touriño, I.; Rojas-Cervantes, M.L.; Gilsanz, M.F.; Gallach-Pérez, D.; Blasco, R.; Barrios-Bermúdez, N.; Cerpa-Naranjo, A. Stability Study of Graphene Oxide-Bovine Serum Albumin Dispersions. *J. Xenobiotics* **2023**, *13*, 90–101. [CrossRef] [PubMed]
26. Xie, Y.; An, J.; Shi, P.; Ye, N. Determinación de lisozima mediante transferencia de energía por resonancia de fluorescencia basada en óxido de grafeno y polietilenglicol. *Anal. Lett.* **2016**, *50*, 148–160. [CrossRef]
27. Liu, Y.; Zhang, Y.; Zhang, T.; Jiang, Y.; Liu, X. Synthesis, characterization and cytotoxicity of phosphorylcholine oligomer grafted graphene oxide. *Carbon* **2014**, *71*, 166. [CrossRef]
28. Zhu, C.; Guo, S.; Fang, Y.; Dong, S.Y. Reducing sugar: New functional molecules for the green synthesis of graphene nanosheets. *ACS Nano* **2010**, *4*, 2429–2437. [CrossRef]
29. Serag, E.; Nemr, A.; El-Maghraby, A. Synthesis of Highly Effective Novel Graphene Oxide-Polyethylene Glycol-Polyvinyl Alcohol Nanocomposite Hydrogel For Copper Removal. *J. Water Environ. Nanotechnol.* **2017**, *2*, 223–234. [CrossRef]
30. Wang, F.; Zhang, P.; Mou, Y.; Kang, M.; Liu, M.; Song, L.; Lu, A.; Rong, J. Synthesis of the polyethylene glycol solid-solid phase change materials with a functionalized graphene oxide for thermal energy storage. *Polym. Test.* **2017**, *63*, 494–504. [CrossRef]
31. Sapsford, K.E.; Tyner, K.M.; Dair, B.J.; Deschamps, J.R.; Medintz, I.L. Analyzing nanomaterial bioconjugates: A review of current and emerging purification and characterization techniques. *Anal. Chem.* **2011**, *83*, 4453–4488. [CrossRef]
32. Cerpa, A.; Lado, I.; Quiroga, O.; Moreno, R.; García, R.; Cerdán, S.; Abu-Lail, N.I. Caracterización coloidal y reológica de SWCNT en medios biológicos. *Int. J. Smart Nano Mater.* **2019**, *10*, 300–315. [CrossRef]
33. Gao, Y.; Wu, J.; Ren, X.; Tan, X.; Hayat, T.; Alsaedi, A.; Cheng, C.; Chen, C. Impact of graphene oxide on the antibacterial activity of antibiotics against bacteria. *Environ. Sci. Nano* **2017**, *4*, 1016–1024. [CrossRef]
34. Singh, V.; Kumar, V.; Kashyap, S.; Singh, A.V.; Kishore, V.; Sitti, M.; Saxena, P.S.; Srivastava, A. Graphene oxide synergistically enhances antibiotic efficacy in vancomycin-resistant *Staphylococcus aureus*. *ACS Appl. Bio Mater.* **2019**, *2*, 1148–1157. [CrossRef] [PubMed]
35. Oves, M.; Rauf, M.A.; Ansari, M.O.; Aslam Parwaz Khan, A.; AQari, H.; Alajmi, M.F.; Sau, S.; Iyer, A.K. Graphene decorated zinc oxide and curcumin to disinfect the methicillin-resistant *Staphylococcus aureus*. *Nanomaterials* **2020**, *10*, 1004. [CrossRef] [PubMed]
36. Bousiakou, L.G.; Qindeel, R.; Al-Dossary, O.M.; Kalkani, H. Synthesis and characterization of graphene oxide (GO) sheets for pathogen inhibition: *Escherichia coli*, *Staphylococcus aureus* and *Pseudomonas aeruginosa*. *J. King Saud Univ.-Sci.* **2022**, *34*, 102002. [CrossRef]
37. Luc, M. A Comparison of Disc Diffusion and Microbroth Dilution Methods for the Detection of Antibiotic Resistant Subpopulations in Gram *Negative bacilli*. Ph.D. Thesis, University of Washington, Seattle, WA, USA, 2015.
38. Saeed, S.I.; Vivian, L.; Zalati CS, C.; Sani NI, M.; Aklilu, E.; Mohamad, M.; Noor AA, M.; Muthoosamy, K.; Kamaruzzaman, N.F. Antimicrobial activities of graphene oxide against biofilm and intracellular *Staphylococcus aureus* isolated from bovine mastitis. *BMC Vet. Res.* **2023**, *19*, 10. [CrossRef] [PubMed]
39. Gayathiri, E.; Bharathi, B.; Priya, K. Study of the enumeration of twelve clinical important bacterial populations at 0.5 McFarland standard. *Int. J. Creat. Res. Thoughts (IJCRT)* **2018**, *6*, 880–893.
40. Hui, L.; Piao, J.G.; Auletta, J.; Hu, K.; Zhu, Y.; Meyer, T.; Liu, H.; Yang, L. Availability of the basal planes of graphene oxide determines whether it is antibacterial. *ACS Appl. Mater. Interfaces* **2014**, *6*, 13183–13190. [CrossRef]
41. Åhman, J.; Matuschek, E.; Kahlmeter, G. EUCAST evaluation of 21 brands of Mueller–Hinton dehydrated media for disc diffusion testing. *Clin. Microbiol. Infect.* **2020**, *26*, 1412-e1. [CrossRef]
42. Zhao, J.; Wang, Z.; White, J.C.; Xing, B. Graphene in the aquatic environment: Adsorption, dispersion, toxicity and transformation. *Environ. Sci. Technol.* **2014**, *48*, 9995–10009. [CrossRef]

43. Bugli, F.; Cacaci, M.; Palmieri, V.; Di Santo, R.; Torelli, R.; Ciasca, G.; Di Vito, M.; Vitali, A.; Conti, C.; Sanguinetti, M.; et al. Curcumin-loaded graphene oxide flakes as an effective antibacterial system against methicillin-resistant *Staphylococcus aureus*. *Interface Focus* **2018**, *8*, 20170059. [CrossRef]
44. Xia, M.Y.; Xie, Y.; Yu, C.H.; Chen, G.Y.; Li, Y.H.; Zhang, T.; Peng, Q. Graphene-based nanomaterials: The promising active agents for antibiotics-independent antibacterial applications. *J. Control. Release* **2019**, *307*, 16–31. [CrossRef] [PubMed]
45. Xu, M.; Zhu, J.; Wang, F.; Xiong, Y.; Wu, Y.; Wang, Q.; Weng, J.; Zhang, Z.; Chen, W.; Liu, S. Improved in vitro and in vivo biocompatibility of graphene oxide through surface modification: Poly (acrylic acid)-functionalization is superior to PEGylation. *ACS Nano* **2016**, *10*, 3267–3281. [CrossRef]
46. Lopez, A.; Liu, J. Covalent and noncovalent functionalization of graphene oxide with DNA for smart sensing. *Adv. Intell. Syst.* **2020**, *2*, 2000123. [CrossRef]
47. Zou, X.; Zhang, L.; Wang, Z.; Luo, Y. Mechanisms of the antimicrobial activities of graphene materials. *J. Am. Chem. Soc.* **2016**, *138*, 2064–2077. [CrossRef] [PubMed]
48. Duch, M.C.; Budinger, G.S.; Liang, Y.T.; Soberanes, S.; Urich, D.; Chiarella, S.E.; Campochiaro, L.A.; Gonzalez, A.; Chandel, N.S.; Hersam, M.C.; et al. Minimizing oxidation and stable nanoscale dispersion improves the biocompatibility of graphene in the lung. *Nano Lett.* **2011**, *11*, 5201–5207. [CrossRef]
49. Liu, J.H.; Yang, S.T.; Wang, H.; Chang, Y.; Cao, A.; Liu, Y. Effect of size and dose on the biodistribution of graphene oxide in mice. *Nanomedicine* **2012**, *7*, 1801–1812. [CrossRef]
50. Singh, S.K.; Singh, M.K.; Kulkarni, P.P.; Sonkar, V.K.; Grácio, J.J.; Dash, D. Amine-modified graphene: Thrombo-protective safer alternative to graphene oxide for biomedical applications. *ACS Nano* **2012**, *6*, 2731–2740. [CrossRef]
51. Dubey, P.; Gopinath, P. PEGylated graphene oxide-based nanocomposite-grafted chitosan/polyvinyl alcohol nanofiber as an advanced antibacterial wound dressing. *RSC Adv.* **2016**, *6*, 69103–69116. [CrossRef]
52. Zhao, R.; Lv, M.; Li, Y.; Sun, M.; Kong, W.; Wang, L.; Song, S.; Fan, C.; Jia, L.; Qiu, S.; et al. Stable nanocomposite based on PEGylated and silver nanoparticles loaded graphene oxide for long-term antibacterial activity. *ACS Appl. Mater. Interfaces* **2017**, *9*, 15328–15341. [CrossRef]